Available online at www.sciencedirect.com
SCIENCE DIRECT
Journal of Colloid and Interface Science 288 (2005) 526–539
JOURNAL OF Colloid and Interface Science
www.elsevier.com/locate/jcis

Prediction of imbibition in unconsolidated granular materials

M. Gladkikh [a], S. Bryant [b,*]

[a] *Institute of Computational and Engineering Sciences, The University of Texas at Austin, 1 University Station CO200, Austin, TX 78712-0227, USA*
[b] *Department of Petroleum and Geosystems Engineering, The University of Texas at Austin, 1 University Station CO300, Austin, TX 78712-0228, USA*

Received 22 January 2004; accepted 11 March 2005

Available online 8 April 2005

Abstract

A new way of modeling imbibition is proposed in this paper. It combines two elements. One is a physically consistent, dynamic criterion for the imbibition of an individual pore originally suggested by Melrose (SPEJ (November 1965) 259–271). The other is the use of a simple but physically representative model of porous media: a dense random packing of spheres that is geometrically predetermined. This approach allows truly a priori predictions of imbibition curves (saturation vs capillary pressure) for different values of contact angle, different initial conditions (e.g., different drainage endpoints), and different macroscopic sample geometries (the ratio of external to internal pores). It also provides a mechanistic basis for understanding the influence of pore-scale phenomena such as "snap-off" of nonwetting phase in the pore throats due to the coalescence of pendular rings. The simulations show that the capillary pressure curve for this unconsolidated packing is very sensitive to the wettability parameters (such as contact angle), whereas the influence of different initial conditions and snap-off is almost negligible. Predicted capillary pressure curves are compared to experimental data presented in the literature, and are consistent with them.

Keywords: Porous media; Imbibition; Finney packing; Snap-off; Meniscus; Residual saturation

1. Introduction

The properties of porous media have a great importance for the modeling and understanding of different flow processes in the subsurface, such as oil recovery, drainage and imbibition, infiltration from surface water, and flow, transport, adsorption and dissolution of contaminants. Because of the great influence of these processes on the environment and industry, there have been numerous attempts to model them at the microscopic scale and to predict the behavior of the subsurface. Many of these attempts model the porous medium as a *network* with *sites* (pore bodies) and *bonds* (pore throats) and some parameters prescribed to the network in advance, for instance, *coordination number* of the sites or *size distribution* of pore bodies and pore throats. By simulating transport processes in such networks one can describe the behavior of the desired unknowns (i.e., relative permeabilities, residual NAPL saturation, dissolution rates, etc.). These network models have been used to study a wide range of the properties in different flow processes, such as relative permeabilities [15,50]; residual nonwetting phase [35]; capillary pressure hysteresis [26,27,31,42]; relationships between capillary pressure, saturation and interfacial areas [6,51]; non-Darcy behavior [62]. Unfortunately, the *predictive* capability of this approach is limited by the presence of prescribed parameters, which usually cannot be determined independently of the phenomena of interest.

The approach considered in this work is similarly devoted to the pore-scale modeling of the flow and transport processes in the subsurface, but it differs significantly from network modeling. The idea is to extract a faithful representation of the actual pore space geometry of a simple but *physically representative* model porous medium [8,10–12,37,38]. The model is a random packing of equal spheres for which the coordinates of the centers have been measured (*Finney pack* [14]). Knowledge of the coordinates completely deter-

* Corresponding author.
E-mail addresses: mgla@ices.utexas.edu (M. Gladkikh), steven_bryant@mail.utexas.edu (S. Bryant).

0021-9797/$ – see front matter
doi:10.1016/j.jcis.2005.03.029

mines the grain space and the void space in the packing. It is also possible to simulate the results of geologic processes in the sphere pack, such as cementation and compaction, thus creating simple models of sedimentary rocks with predetermined pore space geometry [8,10,12].

This class of models has been shown to capture some of the key features of real sediments and sedimentary rocks [7–9,17,37,60]. Other methods of obtaining detailed, realistic, quantitative models of pore space have been developed, along with sophisticated techniques for computing properties of those models [1,3,4,19,28,30,34,47–49,53,54,59,61]. The imbibition mechanism studied here can be applied in any member of this class of geometrically determinate models. Our purpose is to test the macroscopic implications of a pore-level imbibition mechanism. Sphere-pack models are well suited for this purpose. They are a computationally convenient framework for making *a priori* predictions of macroscopic behavior. Because there are no prescribed parameters, testing the predictions against experiments provides physical insight.

If the predictions do not explain experimental observations, we can conclude that the model does not account for some essential aspect of the physical situation, and then seek a more realistic model. On the other hand, a successful prediction allows some confidence that the model can be taken as a reasonable approximation of reality, and thus has a predictive capability and can be used to examine other phenomena. This capability, rather than understanding the behavior of a particular sample(s), is the focus of this paper.

The model of imbibition presented in this paper is based on the methodology developed in [7–9,17,37]. Knowledge of the pore space geometry and wettability conditions (the value of the contact angle, assumed uniform throughout the medium) allows computing the configuration of two fluid phases in porous media under the control of capillary forces. Then the quasi-static imbibition of a wetting phase in this model porous medium is simulated by means of the dynamic Melrose criterion [41]. To our knowledge, this criterion has not been tested in a geometry representative of granular media. An attractive feature of the Melrose criterion is its purely mechanistic nature. Knowledge of grain scale geometry is the only prerequisite for its application. In this way we hope to provide some insight into the long-standing fundamental problem of how imbibition occurs in a single pore. The approach also allows a quantitative understanding of how different macroscopic processes and parameters (for example, capillary pressure–saturation curve) depend on the physical (e.g., wettability) features of porous media during imbibition.

2. Pore-scale description of an unconsolidated medium

In 1899 Slichter [55] suggested the random packing of equal spheres as an “ideal soil.” Though this approach is surely oversimplified, it nevertheless captures many essential features of the pore space of real sediments, Figs. 1 and 2. The most important of these is the randomness in locations of grains, pores and pore throats. Thus, the “ideal soil” model allows constructing simple, but *physically representative* sediments. Moreover, the geometry of pore space is determined by the geometry of the grains making up the porous medium. It is this dependence that enables the successful predictions described above.

Fig. 1. Fontainebleau sandstone.

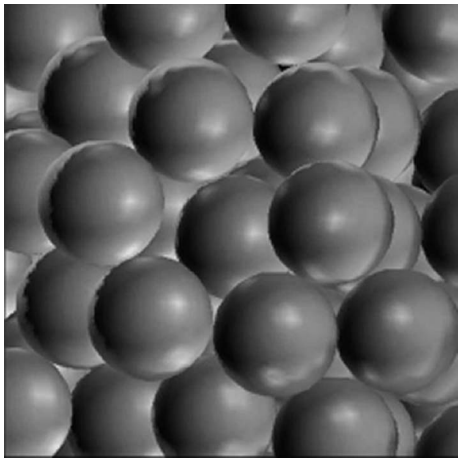

Fig. 2. Random dense packing of equal spheres.

This approach offered useful qualitative insights in the decades after its introduction [18,21–24,56–58]. No quantitative applications involving genuinely random packings were possible, however, until Finney [14] measured spatial coordinates of the centers of about 8000 randomly packed equal spheres, in order to build a model of the liquid state. The power of Finney’s data for the modeling of porous media was quickly recognized and applied by Mason [38]. Later Mellor presented a method (described below) for extracting a network model of the pore space in the Finney packing [39].

The common way of constructing a network model of porous media as a lattice of sites (pores) connected by bonds (pore throats) assumes random assignments of network attributes, such as pore throat and pore body sizes. In real porous media such features are not randomly distributed [8,11] and are difficult to measure. A completely differ-

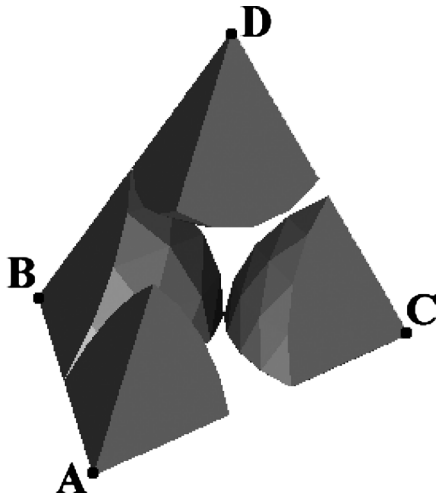

Fig. 3. Tetrahedral cell within the Finney pack, resulting from Delaunay tessellation. The apices of the tetrahedron (points A, B, C, D) are the centers of four nearest neighbor spheres. Only the sections of the spheres contained within the tetrahedron are shown.

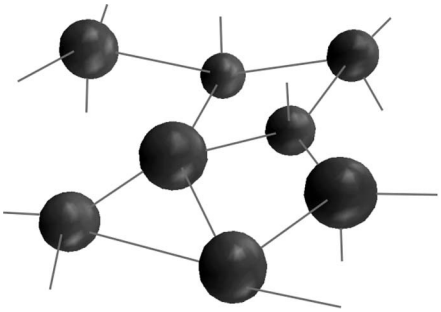

Fig. 4. Schematic representation of a network model. The spheres correspond to the internal regions of tetrahedral cells, Fig. 3, and should not be confused with spherical grains of Fig. 2. The bonds, which connect spheres, correspond to cell faces. Each site has four neighbors.

ent and natural way of constructing a network model from Finney's geometric data is a *Delaunay tessellation* [39] of the sphere centers. Applied to points in n-dimensional space, Delaunay tessellation finds sets of $n+1$ nearest neighbors. Thus it subdivides the volume of the Finney packing into tetrahedra (Fig. 3). Each vertex of the tetrahedron is the center of a sphere. The void space in this tetrahedron corresponds naturally to a pore body. The cross-sectional area of the void goes through a minimum in the plane containing three sphere centers, so the void area in each face of the tetrahedron corresponds naturally to a pore throat.

Thus, a simple network is built (Fig. 4): its "sites" (*pore bodies*, depicted in Fig. 4 as spheres) correspond to the internal regions of tetrahedral Delaunay cells and its "bonds" (*pore throats*, shown in Fig. 4 by lines) correspond to the faces of those cells. (Note that spheres in Fig. 4 are just representations of pore bodies convenient for illustrating network topology; the actual shapes of the pores correspond to the internal regions of Delaunay tetrahedra, shown in Fig. 3. The spheres in Fig. 4 should not be confused with the actual spherical grains, shown in Fig. 2.) All geometrical features of these pore bodies and throats (such as their volume, surface area, etc.) follow directly from the known coordinates of sphere centers. The topology of the network arises naturally: since each cell is a tetrahedron, it has four neighbors, resulting in a lattice of connectivity four. However, the network is completely irregular; there is no evidence of any crystalline structure such as the diamond lattice [39]. In this work the central 3367 spheres of the Finney pack were used, which yield a network with about 15,000 pores and 30,000 pore throats. More detailed description of the Finney pack and the network obtained from it by Delaunay tessellation can be found elsewhere [14,37,38].

3. Model of imbibition

3.1. Capillarity and wetting phase morphology

When viscous and body forces are negligible, the configuration of two fluids is governed by the Young–Laplace [2] equation, which relates capillary pressure to the curvature of the interface between two fluid phases:

$$P_c = \gamma C, \tag{1}$$

where $P_c = P_{NW} - P_W$ is the pressure difference between W (wetting) and NW (nonwetting) phases; γ is the interfacial tension between them and C is the sum of the two principal curvatures, or twice the mean curvature of the interface. In this paper we refer to curvature of the interface, rather than its radii of curvature; the quantities are related by $C = 1/r_1 + 1/r_2$, subject to the usual sign convention for convex and concave sections. In spite of the fact that Eq. (1) describes a static configuration, it is commonly applied to the displacement of one immiscible phase by another, when that displacement occurs sufficiently slowly.

It is assumed during the calculations that W phase in porous medium exists as three different morphologies:

(1) *Pendular rings* (Fig. 5) around *grain contacts*. (In this work, a grain contact is a pair of neighboring spheres, which need not actually touch. W phase supported within the gap between two spheres is often called a *liquid bridge*; for brevity we use the term "rings" to refer to liquid bridges as well.) Pendular rings always exist when two spheres actually touch. If a gap separates two spheres, a pendular ring can exist only at curvatures smaller than a critical value that depends upon the value of the gap between spheres. The geometry of such rings is discussed below;
(2) Completely filled space within a tetrahedral pore. This situation arises during imbibition, when NW phase withdraws completely from a pore, and also during drainage, when W phase can be trapped within the pore [9,45]. In the latter situation the pore remains filled with W phase at any capillary pressure during drainage and contributes to the irreducible W phase saturation;

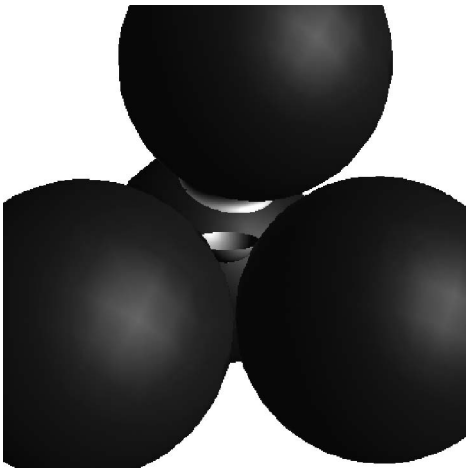

Fig. 5. Four grains and tetrahedral pore, which is formed by them. The light grey shape between the top and rear grains is a pendular ring of W phase, which fills the gap between the grains. The spherical cap in the center of the pore is the interface of the meniscus, which is assumed to have locally spherical shape. Everything below this cap is W phase; above it lies NW phase.

(3) Volume bounded by the *meniscus* in a pore throat that connects an already imbibed pore (completely filled with W phase—case (2)) and non-imbibed pore (which contains NW phase) (Fig. 5). The latter is in this case a natural candidate for the imbibition. The meniscus is assumed to have locally spherical shape. Its geometry is described below.

In this work imbibition is modeled as quasi-static invasion percolation process [63]. The configuration of phases in the beginning of imbibition is taken as the end-point configuration of primary drainage, when irreducible W phase saturation is obtained. This initial configuration is specified by the value of initial curvature and assumes that W phase exists only in the form of pendular rings at grain contacts, where those rings can be supported for the given value of initial curvature. Starting from this initial condition, imbibition proceeds with an incremental decrease of the curvature of the interface. This decrease allows W phase saturation to increase. (In practice, a reduction in *curvature* is achieved by reducing the *capillary pressure*, Eq. (1), and we use these terms interchangeably.)

The algorithm for imbibition proceeds by diminishing the current dimensionless curvature by a small value. Each pore which contains NW phase and is not contained within any cluster of trapped cells (see below) is considered for the pore level events (imbibition and *snap-off* (see below)) that can occur within it. If the Melrose criterion for the imbibition, applied to the given pore, is satisfied, then this pore is checked to determine whether it is contained in a cluster of pores connected to an exit pore. The existence of such a cluster implies a continuous path of pores containing NW phase from the candidate pore to the NW phase reservoir. If this condition is not met, the pore cannot be imbibed; the pore and other pores containing NW phase that are connected to it are added to the list of pores containing *trapped NW phase* (for the implementation of NW phase entrapment see below in the corresponding chapter). Everything within such a trapped cluster of pores becomes frozen, in the sense that all pendular rings and menisci within the cluster cannot change or move. Otherwise, the considered pore becomes imbibed (completely filled with W phase) and menisci arise at all pore throats which connect this pore to non-imbibed neighbors.

Trapped cells and newly imbibed cells are removed from the list of candidates, and this list is re-checked against the criteria for imbibition and snap-off, as described above. When no pore level event (that is, imbibition or snap-off) can happen, it means that an equilibrium configuration has been reached at the current curvature. Then volumes of the phases are computed, which provides the values of phase saturations at current curvature. This completes one iteration of the algorithm, and current curvature can be decreased again.

3.2. Criteria for pore level events

The most important step in the imbibition simulation is to define a *criterion for imbibition* of the given pore. The simplest approach to implement is to assign the value of *critical curvature* for every pore in the packing in advance. W phase is able to invade a pore body only if current curvature of the interface is less than this critical value.

The first attempt to define this critical curvature was made by Haines [22] as

$$C_{\mathrm{H}} = 2/R_{\mathrm{in}}, \tag{2}$$

where R_{in} is the radius of the sphere inscribed into the pore body (such a sphere would touch each of four pore grains).

This so-called *Haines' insphere curvature* would allow *negative hysteresis* for some pores, that is, their critical curvature for drainage would be less than the critical curvature for imbibition [37]. In order to avoid this nonphysical effect, Mason and Mellor [37] proposed to modify the Haines insphere curvature as:

$$C_{\mathrm{MM}} = C_{\mathrm{H}} - 1.6/R_{\mathrm{grain}}, \tag{3}$$

where R_{grain} is grain radius. This empirical modification was specific to a random packing of equal spheres. Eqs. (2) and (3) say that each pore has a fixed, predetermined critical curvature at which it will imbibe. However, there is experimental evidence [31] that the more imbibed neighbors a pore has, the higher the curvature at which it will be imbibed. This contradicts the notion of a predetermined critical curvature for imbibition. Following Jerauld and Salter [27], we can modify the Haines estimate to account for this *dynamic* feature of imbibition as follows:

$$C_{\mathrm{JS}} = C_{\mathrm{H}}/N_{\mathrm{NW}}, \tag{4}$$

where N_{NW} is the number of pores connected to the given pore, which contain NW phase. While qualitatively reasonable, this estimate (Eq. (4)) is essentially empirical.

In this work we apply a different criterion for imbibition, suggested by Melrose [41]. Like the situation described by Jerauld and Salter [27], the *Melrose criterion* is dynamic: we cannot tell in advance the curvature at which each pore is imbibed (though we can enumerate the possible values of this curvature). This criterion will be described in detail below.

Another pore scale event that occurs during imbibition is the *snap-off* of NW phase in pore throats. This can occur in pairs of non-imbibed cells. We apply a mechanistic criterion for snap-off, treating it as the result of *coalescence of pendular rings* (this effect is discussed below). The snap-off at pore throats leads to the formation of lenses of W phase, or double-sided menisci at the pore throats. Subsequently in the simulation, lenses are regarded as a possible source of W phase for the imbibition.

3.3. Boundary conditions for the displacement

In order to simulate imbibition, it is also necessary to define *entrance* and *exit* pores. The entrance pores are assumed to be always connected with the W phase reservoir, and through them W phase invades the packing. The exit pores are assumed to be always connected with the NW phase reservoir and through them displaced NW phase leaves the packing. The pores that are actual surface pores of the Finney packing are natural choices for entrance and exit pores. However, Mason and Mellor [37] have shown that the Finney packing, being a spherical conglomerate, has a high ratio of surface pores to internal pores in comparison with samples typically used in the laboratory. Consequently, simulations in which a large fraction of the surface pores of the Finney pack are taken as W phase entrances do not give a sharp *percolation threshold* (that is, invasion of a large volume of the sample over a narrow range of curvature, once the curvature reaches its specific percolation value). In order to replicate the percolation behavior of real samples, Mason and Mellor [37] proposed to diminish the number of entrance cells, so as to articially reduce the surface area to volume ratio. Using this technique, they obtained percolation threshold at a dimensionless (i.e. for grain radius equal to 1) curvature of about 4.1, which is close to the values observed during experiments. When making a comparison to the experiments, the number of entrance pores can be taken correspondingly to the actual ratio of surface to internal pores in the experimental sample, which is estimated from the grain size and sample geometry. This eliminates the uncertainty in the choice of this parameter, which depends only on the macroscopic geometry of the sample.

As for the exit pores, taking them to be the surface pores of the Finney pack is consistent with most practical situations. The influence of different choices for exit pores (e.g., some fraction of the surface pores, a random selection of pores from within the packing, etc.) on the residual NW-phase saturation is interesting but is beyond the scope of this paper. The choice of the exit pores also depends only upon the geometry of the sample.

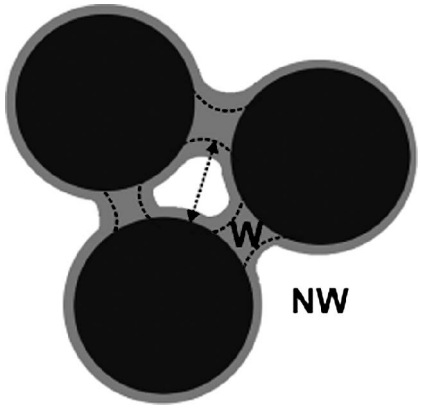

Fig. 6. Influence of W phase connectivity. Pendular rings in the case of disconnected W phase (shown by dotted lines) remain isolated and do not advance within the pore space when curvature decreases. Pendular rings in the case of connected W phase (shown by grey color) are hydraulically connected to the bulk through the thin films around grains and adjust their shape to the current curvature.

3.4. Physical constraints: connectivity of W phase

Another condition of imbibition, which has to be specified, is the *connectivity* of the W phase. If there is a hydraulic conductivity of W phase throughout the whole packing at any stage of displacement, we say the W phase is "completely connected." Here hydraulic conductivity implies that W phase can be moved into any part of the packing instantaneously. At small W phase saturations the movement will require transmission through thin films of W phase on grain surfaces (Fig. 6). Thus it is not trivial to obtain a complete connectivity in practice. The small conductance of films means that the time required for rings to adjust can be quite large.

An important consequence of complete connectivity is that all pendular rings in the packing are surfaces of curvature equal to the currently applied value. Thus they adjust their shape immediately when a change in the capillary pressure is applied. In particular, all the rings will grow and advance along grain surfaces as the curvature decreases during imbibition. The converse holds during drainage. Complete connectivity is thus a limiting case. This model of "complete connectivity" uses thin films as a proxy for all subgrain-scale features that could act as conduits for W phase. That is, we do not resolve surface roughness, individual channels on grain surfaces, etc., but we do account for their collective effect on the imbibition process.

On the other hand, if W phase does not possess complete connectivity, then a pendular ring becomes "trapped" during drainage (that is, loses its connection to the bulk volume) and remains a surface whose curvature is held constant at the value at which it was trapped. (For convenience in treating trapped volumes we have assumed incompressible phases and zero interphase mass transfer.) The trapped ring contributes to the irreducible wetting phase saturation. If imbibition starts from this drainage endpoint, such a ring cannot grow until it becomes connected to the bulk volume of W

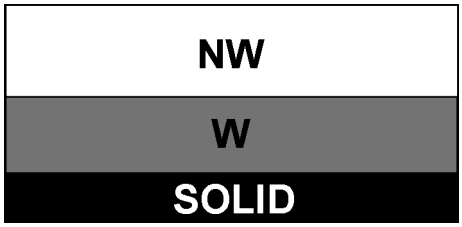

Fig. 7. Spreading of the W phase upon the solid surface (the contact angle of W–NW–solid interface is zero).

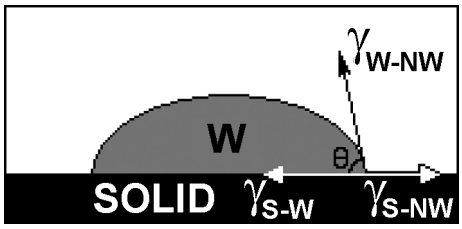

Fig. 8. Formation of a drop of W phase on the solid surface. The contact angle of W–NW–solid interface has non-zero value θ.

phase again. Such re-connection happens when the W phase imbibes pores neighboring to this ring. So, the existence of thin films on grain surfaces causes qualitatively different behavior during displacement processes. Different configurations of the system for both cases of W phase connectivity are shown in Fig. 6. Pendular rings for the case of the disconnected W phase (shown by dotted lines) remain isolated and do not advance within the pore space; whereas for the case of the connected W phase (shown by grey color) they are hydraulically connected to the bulk of W phase through the thin films and adjust their shape to the current capillary pressure.

3.5. Physical constraints: wettability

The condition of W phase connectivity arises naturally from the *wettability* of the system, specified by the value of *contact angle* θ. Namely, if the W–NW–solid contact angle is zero, then W phase spreads upon the grain surface (Fig. 7) and thus thin film is formed (this follows from the Young–Dupre contact angle equation [2]). If the contact angle has non-zero value, then such a film cannot be formed and the drop of W phase arises instead on the grain surface (Fig. 8). All other values of contact angle, different from zero, result in a qualitatively similar behavior of the system. The only change is in the local geometry of the phases (i.e. menisci and pendular rings).

The implications of this model for a perfectly wetted surface (zero contact angle) are that wetting phase exists as a film on grain surfaces and occupies all grooves, micropores, etc. In particular, this is the case at the beginning of the imbibition simulation, which we take to be the endpoint of a drainage displacement (large but finite value of capillary presure.) This is the rationale for not modeling grain roughness explicitly, as described above.

4. Pendular rings at grain contacts

Pendular rings play a crucial role in this approach to simulating imbibition. Indeed, when W phase saturation is small (early stages of imbibition or late stages of drainage), the W phase exists mostly in the form of such rings, which occupy the space between solid grains (Fig. 9). Moreover, their geometry is an essential part of the Melrose imbibition criterion. Quantifying their shape as a function of curvature in some detail is therefore necessary.

This is one of the classical problems concerning the configuration of a mass of liquid which exists in a gap between two solid surfaces, formulated first by Plateau [46]. Knowing all geometric features of such rings, we can include their contribution to imbibition or drainage capillary pressure curves (since the curvature defines capillary pressure and total volume of rings defines W phase saturation). We also need to investigate the stability of these rings for two situations: when they are isolated, and when they come in contact with other interfaces. This will establish the basis for the different pore level physical events that happen as a result of the intersection of the interfaces.

Grain particles are assumed to be equal spheres with radius R (Fig. 9). The known values are the gap h (half of the distance between spheres, readily determined from the known locations of the spheres) and the current curvature C of the liquid bridge surface (since the curvature (or pressure) controls imbibition and can be measured). In the Finney packing, about half the pairs of nearest neighbor grains are in contact, in which case $h = 0$. One way to solve this problem is to approximate the liquid bridge as a surface of revolution of a circular arc—*toroidal* approximation [23]. This approximation admits an analytical solution (i.e. equation for the shape of the ring) for the given h and C. Formulas for $h = 0$ can be found, for example, in [20,40,52] and for $h > 0$ in [29].

The true form of the ring is not toroidal, but can be found from the fact that its surface must have constant curvature everywhere. The latter condition produces a surface known as the *nodoid*. Obtaining the features of such a body is not simple and demands numerical solution of differential equa-

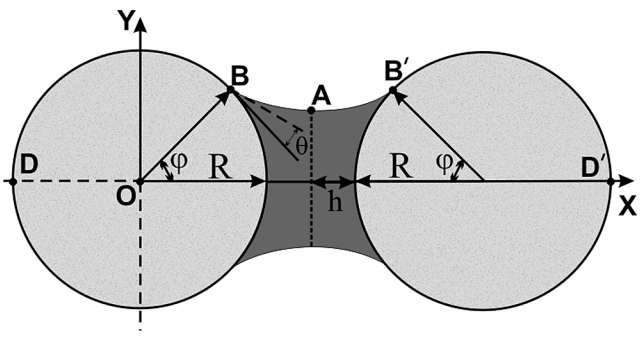

Fig. 9. Pendular ring between two equal spheres; we use the term to denote liquid bridges as well as rings. θ—contact angle; φ—filling angle; h—half the gap between spherical grains.

tions (Eq. (5)). For the case $h = 0$ these calculations were thoroughly made by Fisher [16], who has found errors due to simplified toroidal approximation, and later by others such as Erle et al. [13], Lian et al. [33], etc. They showed that the error of the toroidal approximation is no more than 1.5% for liquid neck (which is equal to Y_A in Fig. 9) and no more than 5% for the volume of the ring. Thus, for the case of $h = 0$ the toroidal approximation is adequate for the purposes of simulating imbibition. For $h > 0$, however, the error in the toroidal approximation becomes large (see below), and the nodoid solution is required.

Numerical solutions for the case $h > 0$ were found by several authors [13,33] who examined the behavior of the liquid drop of fixed volume for different separations s (*separation* is defined as $s = R + h$). For a given separation s and fixed volume there are two possible curvatures of the ring. This also tells that at a given curvature and separation there is a range of possible volumes of the bridge. Unfortunately, in the drainage or imbibition simulation, the volume of the ring is unknown and must be found from the given separation and curvature. The possibility of existence of different bridge volumes (and, thus, bridge shapes) can be overcome by choosing the shape which provides the minimal surface area of the pendular ring (this shape will be preferable from the physical point of view, since in the situation of the dominance of the capillary forces, surface area corresponds to the free energy of the system). Mathematically it means that we need to minimize the free energy functional with the constraint on some other parameters (gap distance, volume, etc.) that define the corresponding parametrical space of equilibrium shapes of the liquid bridge.

This approach leads to the following Euler–Lagrange equation [13]:

$$\dot{Y} = -\sqrt{\frac{4Y^2}{(K - CRY^2)^2} - 1}. \tag{5}$$

This equation is integrated for chosen values of curvature C and filling angle φ. Boundary conditions at the point B are specified by filling angle φ and contact angle θ:

$$X_B = R\cos\varphi, \quad Y_B = R\sin\varphi, \quad \dot{Y}_B = \cot(\varphi + \theta). \tag{6}$$

Integration is stopped when the boundary condition at the point A is met, that is, $\dot{Y} = 0$.

Eq. (5) was integrated numerically in its dimensionless form, that is, for $R = 1.0$. For the numerical integration of (5) the predictor–corrector scheme was used, with the explicit Euler method as the predictor and the trapezoidal rule as the corrector. The step-size in X direction was chosen to be 10^{-5} to ensure stability of the numerical method.

This technique allows finding the point A as the point where the integration is stopped. In the context of Fig. 9, this is equivalent to finding the separation s for the given values of the curvature and filling angle. Unfortunately, in the drainage or imbibition simulation we are given the values of curvature and separation, and the problem is to compute the value of the filling angle. To resolve this inverse problem, we need to integrate (5) for the whole range $(0, \pi/2)$ of filling angles and find the solution which corresponds to the given separation.

In order to find the set of solutions corresponding to the given values of curvature and separation, we compute first a map of solutions to the Euler–Lagrange equation (5) for a rectangular grid of values of C and φ. Values of C in the range $(0, 20)$ with the increment of 0.1 and values of φ in the range $(0, \pi/2)$ with the increment 0.005 were used.

Fig. 10 represents the set of solutions to the liquid bridge problem as curves of constant separation, that is, the relationship between filling angle φ and curvature C of the liquid bridge surface for the fixed value of separation s. Solutions for both toroid and nodoid are shown. Fig. 10 illustrates the fact that for any separation greater than unity there exists a *critical curvature* for stability of the bridge. For values of

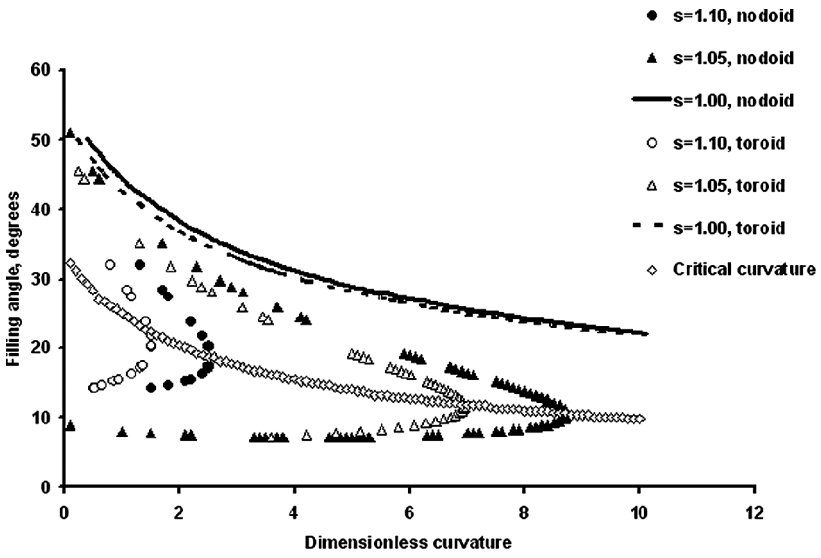

Fig. 10. Curves of constant separation in filling angle–curvature space. Solutions for both true shape of nodoid and toroidal approximation. Contact angle is zero.

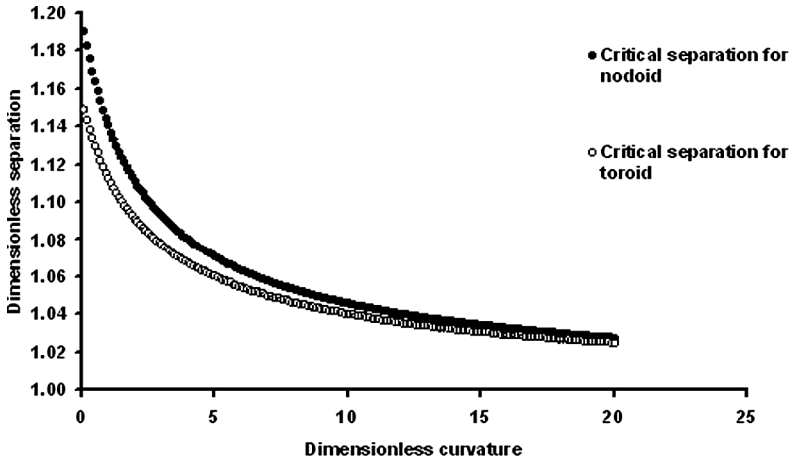

Fig. 11. Critical separation as a function of curvature. Contact angle is zero.

curvature greater than this critical value the liquid bridge does not exist. For values of curvature less than the critical value, there are two solutions (two different values of filling angles), one of which (the smaller filling angle—lower branch of the curve) we consider to be mechanically unstable. This instability is confirmed by the experimental data [13,36].

In Fig. 10 curves for the toroidal approximation are presented also. The error associated with this approximation is very small for the curve with $s = 1.00$ (spheres in contact) but increases with an increase in s and is larger for the values of curvatures near the critical. Knowing whether a bridge exists at a given grain contact is of obvious importance in imbibition simulations. It is convenient to summarize the locus of critical points from Fig. 10, and this is done in terms of separation and curvatures in Fig. 11. The curves in Fig. 11 show that the toroidal approximation underestimates the value of critical separation for the given curvature and also the value of the critical curvature for the given separation. That is, the nodoid still exists (is stable) at the values of curvatures and separations, where the toroid breaks (is unstable).

5. Coalescence of pendular rings

To this point we have considered the liquid bridge in isolation. In dense packings of equal spheres, the average sphere has approximately eight contacts that will support pendular rings [5]. The presence of multiple rings on a single sphere raises the possibility of *coalescence*—intersection of two or more distinct rings which then merge—as the volume of the rings increases during imbibition. When this occurs on the three spheres defining a pore throat, it is often called *snap-off* of NW phase, because it leads to full closure of pore throats (bonds of the network—faces of tetrahedral cells) with W phase. The stages of coalescence of pendular rings are shown in Figs. 12 and 13.

This effect was thoroughly analyzed by Haines [24]. Consider three spherical grains, which are in point contact with each other. There will be three pendular rings at grain contacts. With decreasing curvature (and, thus, increasing W phase saturation) pendular rings grow and at some point they will just touch each other (Fig. 12). This leads to the mechan-

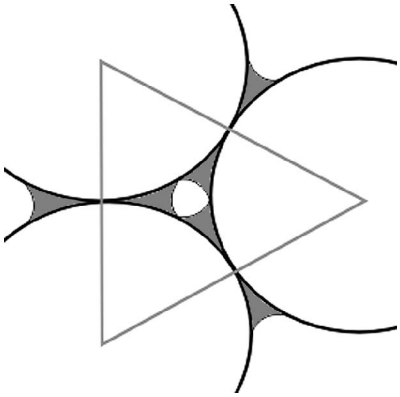

Fig. 12. Initial stage of coalescence. 2D slice of the pore throat by the plane that contains grain centers. The pore throat is the void area within the face of a Delaunay tetrahedron, shown by the grey triangle. Three pendular rings just touch each other. W phase is shown by grey color; NW phase—by white in the middle of the pore throat.

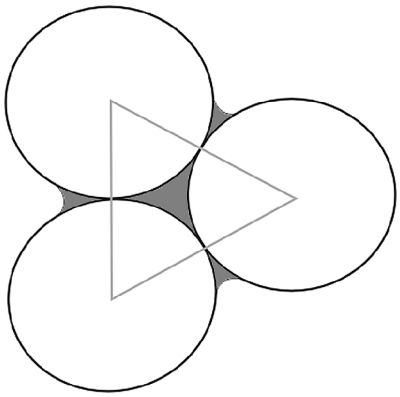

Fig. 13. Final stage of coalescence. Pore throat is full of W phase. The NW phase previously connected via the white "hole" between the rings in Fig. 12 has been "snapped off."

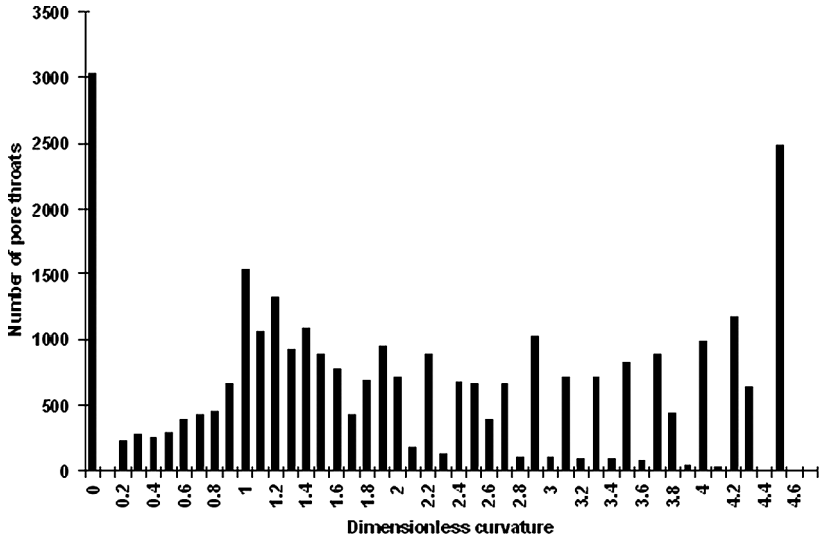

Fig. 14. Distribution of the a priori dimensionless coalescence curvatures for the pore throats in the Finney packing for zero contact angle. Maximal possible coalescence curvature of about 4.5 corresponds to the case of three grains in actual contact with each other.

ical instability of the interface. The rings will spontaneously coalesce, which, in turn, leads to the complete filling of the pore throat by W phase, causing snap-off of NW phase. At this final stage of coalescence the pore throat is full of W phase, which is shown in Fig. 13, and the previously continuous volume of NW phase now exists in two distinct blobs (not shown).

Using exact calculations of ring geometry described above, it is straightforward to obtain the *coalescence curvatures* for each pore throat in the packing, i.e. curvatures at which neighboring pendular rings will coalesce. The distribution of dimensionless coalescence curvatures for the case of zero contact angle is shown in Fig. 14. The case with three grains in actual contact with each other provides the pore throat with the highest possible coalescence curvature. For the case of zero contact angle the value is about 4.5. Not all throats in the model porous medium are formed by three spheres in contact; most in fact have gaps between at least one pair of spheres. The range of relative locations of pore-throat-defining spheres accounts for the distribution in Fig. 14.

These coalescence curvatures have a priori character. That is, they are obtained *independently* of the actual sequence of pore-level imbibition events, and thus represent the properties of the pore throats only.

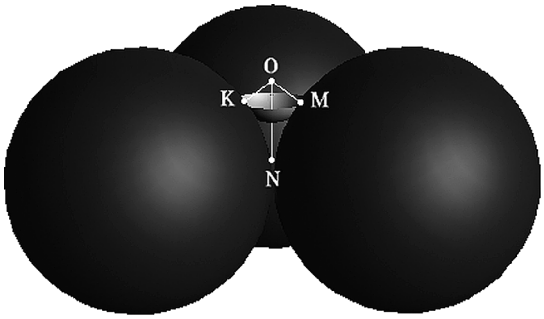

Fig. 15. Pore throat, formed by three grains, which contains meniscus between W and NW phases. The meniscus is assumed to have *locally spherical shape* (spherical cap). N is the point equidistant from the grain centers and lying in the same plane as those centers. Vector ON is perpendicular to this plane. Point O is the center of the meniscus sphere. W phase occupies pore space below the cap; NW phase above.

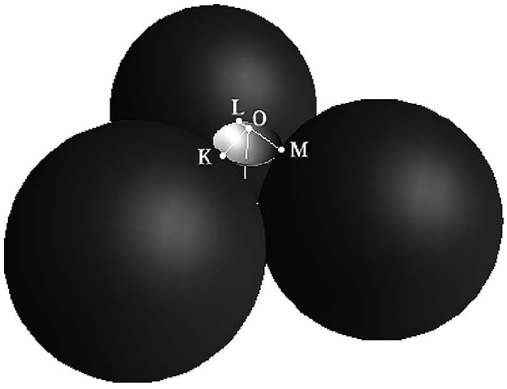

Fig. 16. Another point of view to the meniscus, shown on Fig. 15. Meniscus touches grain spheres at points K, L and M.

6. Menisci between phases

When W phase penetrates into the packing, it completely fills some of the pores. In the throats, which connect already imbibed pores (filled with W phase) with non-imbibed ones (filled with NW phase), the interface between phases appears in the form of a *meniscus* (Figs. 5, 15 and 16).

W phase occupies the pore space below the meniscus pictured in Figs. 15 and 16. The meniscus extends into the volume between each pair of grains. In fact, in the immediate vicinity of the grain contacts, the shape of the meniscus will resemble a liquid bridge. Far from the contacts in the vicinity of center of the pore throat, we assume that the meniscus

has locally spherical shape. That is, the meniscus is assumed to be a segment of a sphere (spherical cap) whose radius corresponds to the current curvature C of the interface (Figs. 15 and 16):

$$R_{\text{men}} = 2/C. \tag{7}$$

The actual meniscus shape will be a hybrid of the spherical cap and the pendular ring. The approximation of Eq. (7) avoids the difficulty of computing the true shape; it is reasonable except at small curvatures (approaching residual NW saturation) when it leads to overlap of pairs of menisci in some pores.

The calculations of the geometry of such locally spherical meniscus are as follows. We define point N (Fig. 15) from two conditions. First, it lies in the plane defined by the centers of three grains, which form the given pore throat. Second, it is equidistant from the centers of these three grains. Then, the center of the spherical cap (point O in Fig. 15) must lie on the line which contains point N and is perpendicular to the plane of the pore throat containing N.

Knowing the line ON and the radius of the meniscus' sphere, determined by Eq. (7), we can find the coordinates of the point O from the condition that the meniscus' sphere intersects these three grains at an angle equal to the specified contact angle (points K, L and M in Fig. 16). Thus, the meniscus has a dynamic behavior, that is, its shape and location change as curvature changes.

The subsequent computation of the volume of W phase in the pore throat below the meniscus is straightforward, though tedious.

7. Melrose criterion for the imbibition of a pore

We are now ready to describe the most important step in the simulation of imbibition, the definition of the criterion for imbibition within a given pore. We use a dynamic approach proposed by Melrose [41]. Having computed the geometry and location of every pendular ring and meniscus in the packing for the given value of current curvature, we determine the configuration of W phase within every pore. The simplest possible configuration in a pore is depicted in Fig. 17: a meniscus is present in one pore throat, and one grain contact not associated with that throat supports a pendular ring. If the curvature is decreased, both the pendular ring and the meniscus grow and advance into the pore space. Their new locations follow from the calculations described above. Further decreases in curvature cause further growth and advance, until at some value of curvature the meniscus and ring touch at some point J (Fig. 18) on the surface of the corresponding grain. An infinitesimal decrease in curvature leads to the mechanical instability of the interface, which, in turn, results in the imbibition event: the ring and meniscus merge to form a single surface, and the NW phase

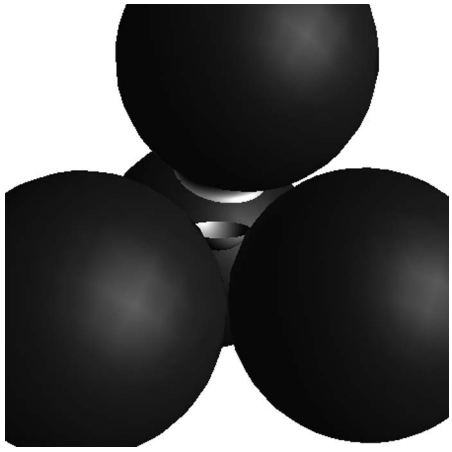

Fig. 17. Illustration of Melrose criterion for imbibition. The simplest configuration of fluids in a non-imbibed pore is shown. The value of curvature is fixed. A meniscus has reached a stable position in the pore throat formed by three lower grains. A pendular ring is supported at the contact between upper and rear grains. At this value of curvature, the ring and meniscus are separate, independent bodies.

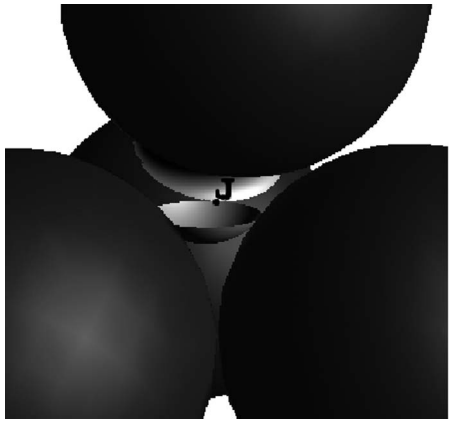

Fig. 18. At a smaller value of curvature than in Fig. 17, the ring and meniscus first come into contact at point J. This results in the instability of the interface and leads to the imbibition event: all NW phase withdraws and W phase completely fills the pore.

spontaneously withdraws from the pore, leaving W phase completely filling the pore.

The extension of this idea to the other possible meniscus/pendular ring configurations in a pore is straightforward. At a given curvature and for a given pore, we catalog all the menisci and rings in that pore. For each meniscus, we test for contact with independent rings (i.e., rings held at grain contacts not associated with the pore throat containing the meniscus). If any of the tests are positive, then the Melrose criterion is satisfied. The pore is then allowed to imbibe as described in Section 3.

8. Entrapment of NW phase

During imbibition, NW phase can be *trapped* inside the pore bodies, which results in the *residual NW phase satura-*

tion at the end of the imbibition (at zero curvature of bulk W phase). The structure and magnitude of this residual saturation are very important and demand separate discussion. NW phase can be trapped in one pore body or in several neighboring pore bodies (*trapped cluster of pores*) due to the loss of connectivity with the exit pores, i.e. with the pores assumed to be connected to the NW phase reservoir. In Fig. 19, one possible way of entrapment of NW phase is represented. In this figure W phase is shown by black color and NW phase by grey. In configuration I the central and upper pores are not imbibed yet and contain NW phase. Suppose that the upper cell has an exit pore as a neighbor, so NW phase in configuration I is connected to the NW phase reservoir and thus is not trapped. Suppose further that the imbibition event, according to the Melrose criterion, occurs first in the upper pore (with the meniscus advancing from the pore, containing W phase, from the right—direction of this movement is shown in Fig. 19 by black arrow). At the same time NW phase in the upper pore retreats into NW phase reservoir (the direction of this movement is shown in Fig. 19 by grey arrow). At the moment, when this upper pore is imbibed, the central pore loses its connection to the NW phase reservoir and becomes trapped, configuration II.

Thus, using the strategy for the entrapment, described above, we obtain residual NW phase distribution.

9. Results and discussion of imbibition simulation

Simulations of imbibition in the Finney packing were conducted with the algorithms described above. Fig. 20 presents the results of these simulations for different wettability conditions (different values of contact angle) and also shows the influence of coalescence. During the simulations shown in Fig. 20, the number of entrance pores chosen was 187 (which is about 10% of the actual surface pores of the Finney pack and corresponds roughly to the geometry and size of the sample, used in the experiments of Haines [24]—see below). All the actual surface pores of the packing were chosen as exit pores (that is, connected with NW phase reservoir).

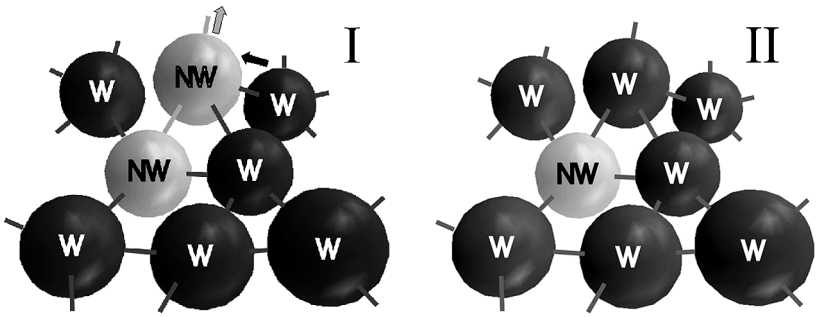

Fig. 19. One of possible ways of entrapment of NW phase. In configuration I, both pores containing NW phase are connected to the reservoir of NW (not shown). An imbibition event occurs in the upper pore containing NW phase before the central pore. Thus it imbibes first, in this case with the meniscus advancing from the pore, containing W phase, at the right. The direction of the W phase meniscus movement is shown with black arrow. NW phase in the upper pore retreats into NW phase reservoir—the direction of this movement is shown with grey arrow. Thus NW phase in the central pore becomes trapped, configuration II. This is the situation for most of the residual NW saturation, though many clusters of several pores containing NW also get trapped.

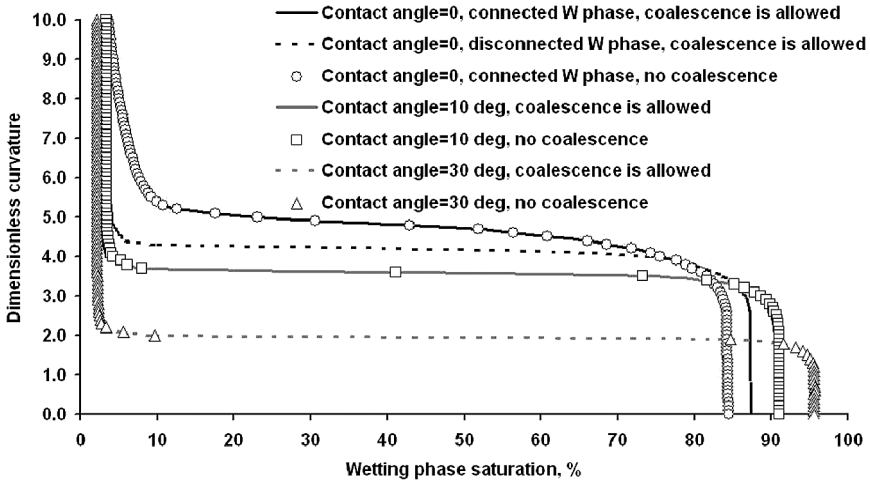

Fig. 20. Simulations of imbibition in the Finney pack. Increasing the contact angle reduces the curvature at which percolation occurs and reduces residual NW saturation. In this unconsolidated medium, coalescence of pendular rings (snap-off) does not affect the macroscopic behavior.

9.1. Effect of contact angle

Fig. 20 illustrates strong dependence of the imbibition on the wettability of the packing. W phase connectivity is also important. Two curves with the same value of contact angle, equal to zero, but different W phase connectivity exhibit a shift of about 1 dimensionless unit of curvature. The curve for zero contact angle with disconnected W phase is intended as a limiting case. It corresponds to two possible situations. In one, the wetting phase films on grains do not allow the movement of W phase on the time scale of the experiment. That is, the time interval between increments in the curvature is long enough for the bulk W phase to imbibe from one pore to the next, but too short for appreciable flow through thin films. In the other, thin films are absent from grain surfaces and contact angle is finite but not experimentally distinguishable from zero.

At larger values of contact angle, W phase can become completely disconnected, because thin films cannot be formed. Larger contact angles lead to smaller imbibition curvatures, and the percolation threshold in the imbibition curve shifts to smaller curvatures. Another effect of the increasing value of contact angle is the *decrease* of the value of residual NW phase saturation. There are two causes for this decrease: (1) the decrease in the *number fraction* of the pores which contain residual NW phase, and (2) the increase in the volume of W phase, neighboring to the trapped pores. The reason for the latter is that, since for the higher contact angles imbibition happens at lower curvatures, menisci and pendular rings can grow further into the pore space and occupy more pore volume.

9.2. Effect of snap-off

Since coalescence of pendular rings leads to the closure of pore throats to NW phase, it diminishes NW phase connectivity, which should increase the likelihood of entrapment of NW phase. This qualitative argument has led to the conventional wisdom that these snap-offs are a key mechanism affecting the value of residual NW phase saturation. But the results of simulations presented in Fig. 20 show that in an unconsolidated bead pack snap-off has negligible effect for any value of contact angle. This is readily explained by comparing the values of coalescence curvatures to the curvatures at which the main portion of imbibition events happens. The distribution of coalescence curvatures was shown in Fig. 14 for zero contact angle. No coalescence can occur until the curvature falls to about 4.5. But the percolation threshold for imbibition at zero contact angle is at a curvature of about 5, Fig. 20. Thus, when the curvature becomes small enough for coalescence to happen, most pores in the packing are already imbibed or trapped, and few throats will contain NW phase. Thus the effect of coalescence on the imbibition curve is imperceptible. This conclusion is specific to unconsolidated packings; in future publications, we will describe its role in consolidated materials.

9.3. Comparison of predictions and experiments

The comparison between predicted capillary curves and experimental data is presented in Fig. 21. The predictions were made with conditions consistent with those reported for the experiments. Initial dimensionless curvature equals 10; value of contact angle is zero; number of cells connected with W phase reservoir is 187; actual surface cells of Finney packing were taken as exits in order to define trapping criterion for NW phase. In this initial state, W phase was taken to exist only as pendular rings at the initial curvature.

For the comparison, we took data from the classical works of Haines [24] and Leverett [32]. Haines performed imbibition experiments in “glistening dew,” glass beads of diameter 0.38 mm. He observed thin films on grain surfaces,

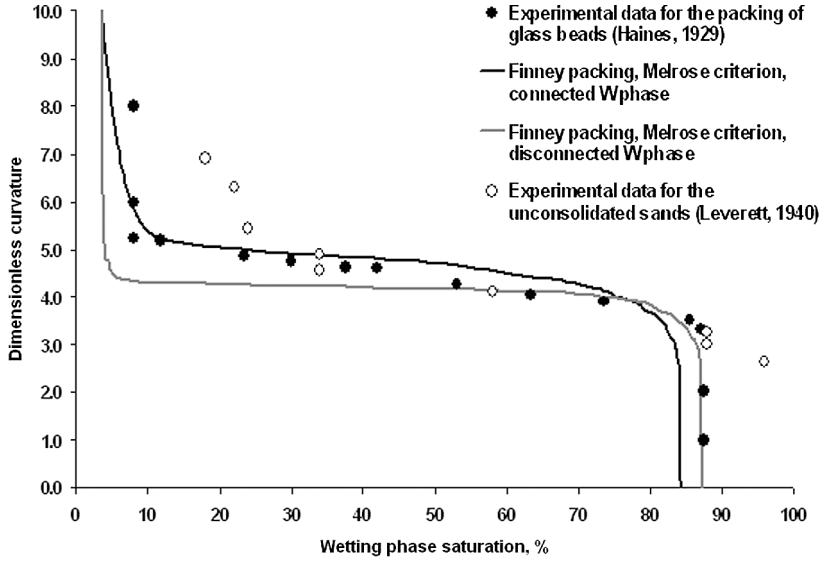

Fig. 21. Comparison between predicted imbibition capillary curves and experimental data.

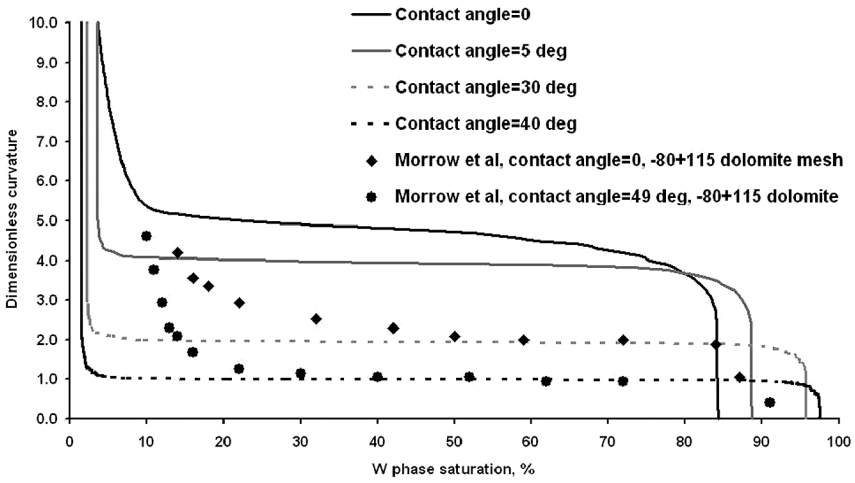

Fig. 22. Influence of wettability. Comparison between predicted imbibition capillary curves and experimental data.

indicating the value of contact angle was zero, though the hydraulic conductivity of these films is unknown. The ratio of entrance to internal pores in the sample was about 0.1 (which is taken as the ratio of surface to volume grains in the sample); we took the same ratio of pores for the Finney packing in our simulations. Fig. 21 shows good agreement between prediction and experimental data by Haines. In order to estimate the influence of hydraulic conductance of thin films on grain surfaces, two predicted curves are shown in Fig. 21: one for the complete W phase conductivity and the other for the case of completely disconnected W phase (as discussed above, both curves are for zero contact angle).

From Fig. 21 we can see that Haines' data generally fall in between those two predicted curves. This suggests the connectivity of W phase during the experiment was intermediate between the two extremes modeled. A possible physical interpretation is that when bulk W phase advances to within a short distance from a pendular ring (but does not touch it), flow through thin films is fast enough to connect the pendular ring to the bulk W phase. Thus at each step of the imbibition, a fraction of the rings would adjust their shape to the current curvature. For the upper curve in Fig. 21, all the rings adjust their shape; for the lower curve, none do.

Data from Leverett [32] for unconsolidated sand are also shown in Fig. 21. Though we do not know wettability conditions during the experiment, his experimental points fall closely both to the predicted curves and data from Haines' experiments, which also supports the presented approach.

The predicted influence of wettability on the imbibition capillary curves, shown in Fig. 20, needs to be compared to that observed during experiments performed in media with independently measured value of contact angle. Such a comparison is shown in Fig. 22. Presented in this figure are the predicted curves for different values of contact angle and experimental curves, obtained by Morrow et al. [44] for the water–decane imbibition in a sample of crushed dolomite. The wettability (value of advancing contact angle) in their experiments was controlled by the concentration of octanoic acid in the decane (which was a nonwetting phase).

Pore dimensions in the crushed dolomite evidently differ from those in a random packing of spheres of comparable size, perhaps due to the angularity of the dolomite. Drainage in their experiments occurred at the dimensionless curvature of about 4, a substantially smaller value than in the random sphere packs (see, for example, [9]). Similarly, the predicted imbibition curve for zero contact angle is at a larger dimensionless curvature than the experimental one. Nevertheless, qualitative comparison can be done. In Fig. 22 the experimental curves shift down to the smaller curvatures at the larger contact angle, similar to the shift in the predicted curves. Traditional applications of the law of capillarity would predict a shift directly proportional to the ratio $\cos\theta_1/\cos\theta_2$. The observed shift is much larger and is similar to the predicted shift. This result strongly supports the validity of the Melrose criterion for imbibition. Other criteria that depend on pore geometry (Haines' insphere [22], Eq. (2); Mason and Mellor [37], Eq. (3)) will vary essentially linearly with $\cos\theta$. Moreover, the smaller value of the residual NW phase saturation at higher contact angle is also consistent with the predictions. The results of other experiments, obtained for different types of porous media (Morrow and Mungan [43] (teflon), Harris et al. [25] (crushed galena)) also qualitatively support the predicted influence of wettability.

10. Conclusions

In this work we present a method of simulating wetting phase imbibition using a physically consistent dynamic criterion for the imbibition of a single pore. Originally proposed by Melrose [41], the criterion is purely geometrical and thus allows a priori predictions of imbibition curves. Moreover, the influence of different conditions and physical phenomena, such as wettability, hydraulic continuity of wetting phase and coalescence of pendular rings (snap-off), can be predicted quantitatively. We illustrate these influences in a simple unconsolidated porous medium the detailed geom-

etry of which is already known. Hydraulic continuity and coalescence affect predicted capillary curves only slightly. The Melrose criterion leads to a stronger dependence on wettability (nonlinear in cosine of the contact angle) than expected from usual applications of the law of capillarity. It also predicts that the magnitude of residual NW phase saturation decreases as contact angle increases. Experimental data presented in the literature are consistent with all these predictions. We conclude that the Melrose criterion reflects the relevant physical processes during imbibition in an unconsolidated medium, and that it therefore warrants further testing in geometrically detailed descriptions of other types of porous media.

Acknowledgments

Funding for the work reported in this paper was provided by UT Austin's Research Consortium on Formation Evaluation, jointly sponsored by Baker Atlas, Halliburton, Schlumberger, Shell International E & P, and Anadarko Petroleum Corporation. The support for the first author was also provided by National Water Research Institute. This material is also based in part upon work supported by the Texas Advanced Technology Program under Grant No. 003658-0408-2003.

The contents do not necessarily reflect the views and policies of the sponsors nor does the mention of trade names or commercial products constitute endorsement or recommendation for use. This paper has not been subject to agency review and therefore does not necessarily reflect the views of the sponsoring agencies, and no official endorsement should be inferred.

We are grateful to Prof. Finney for the access to his sphere packing coordinates.

References

[1] A. Al-Futaisi, T.W. Patzek, Water Res. Research J. 39 (2) (2003) 1042–1055.
[2] A.W. Adamson, Physical Chemistry of Surfaces, Wiley, New York, 1990.
[3] S. Bakke, P.E. Øren, SPEJ 2 (1997) 136–149.
[4] B. Berkowitz, D. Hansen, Transp. Porous Media 45 (2001) 303–319.
[5] J. Bernal, J. Mason, Nature 188 (1960) 910–911.
[6] S.A. Bradford, F.J. Leij, J. Contam. Hydrol. 27 (1997) 83–105.
[7] S.L. Bryant, M. Blunt, Phys. Rev. A 46 (1992) 2004–2011.
[8] S.L. Bryant, C. Cade, D. Mellor, AAPG Bull. 77 (8) (1993) 1338–1350.
[9] S.L. Bryant, A.S. Johnson, Chem. In. Env. ACS Symp. Ser. 806 (2001) 26–41.
[10] S.L. Bryant, P.R. King, D.W. Mellor, Transp. Porous Media 11 (1993) 53–70.
[11] S.L. Bryant, G. Mason, D. Mellor, J. Colloid Interface Sci. 177 (1996) 88–100.
[12] S.L. Bryant, D.W. Mellor, C.A. Cade, AIChE J. 39 (1993) 387–396.
[13] M.A. Erle, D.C. Dyson, N.R. Morrow, AIChE J. 17 (1971) 115–121.
[14] J.L. Finney, Proc. R. Soc. London Ser. A Math. Phys. Sci. 319 (1970) 479–493.
[15] U. Fischer, M. Celia, Water Res. Research J. 35 (1999) 1089–1100.
[16] R.A. Fisher, J. Agric. Sci. 16 (1926) 492.
[17] M. Gladkikh, S. Bryant, Adv. Water Res. 26 (2003) 609–622.
[18] L. Graton, H. Fraser, J. Geology 43 (1935) 785–909.
[19] D. Grunau, S. Chen, K. Eggert, Phys. Fluids A 5 (1993) 2557–2562.
[20] H. Gvirtzman, P.V. Roberts, Water Res. Research 27 (6) (1991) 1165–1176.
[21] F.E. Hackett, J.S. Strettan, J. Agric. Sci. 18 (1928) 671–681.
[22] W.B. Haines, J. Agric. Sci. 20 (1930) 97.
[23] W.B. Haines, J. Agric. Sci. 15 (1925) 529–535.
[24] W.B. Haines, J. Agric. Sci. 17 (1927) 264–290.
[25] C.C. Harris, A. Jowett, N.R. Morrow, Trans. Inst. Min. Metall. 73 (5) (1963–1964) 335–351.
[26] R.J. Held, M.A. Celia, Water Res. Research 37 (1) (2001) 165–170.
[27] G.R. Jerauld, S.J. Salter, Transp. Porous Media 5 (1990) 103–151.
[28] G. Jin, T.W. Patzek, D.B. Silin, Physics-Based Reconstruction of Sedimentary Rocks, SPE 83587, SPE Western Regional/AAPG Pacific Section Joint Meeting, Long Beach, CA, 19–24 May, 2003.
[29] A.S. Johnson, Pore Level Modeling of Interfacial Area in Porous Media, M.S. Thesis, The University of Texas at Austin (2001).
[30] R. Knight, A. Chapman, M. Knoll, J. Appl. Phys. 68 (1990) 994–1001.
[31] R. Lenormand, C. Zarcone, Role of Roughness and Edges during Imbibition in Square Capillaries, SPE Paper 13264.
[32] M.C. Leverett, AIME Pet. Trans. (1941) 142.
[33] G. Lian, C. Thornton, M.J. Adams, J. Colloid Interface Sci. 161 (1993) 138–147.
[34] W. Lindquist, A. Venkatarangan, J. Dunsmuir, T.-F. Wong, J. Geophys. Res. 105 (2000) 21508–21528.
[35] M.I. Lowry, C.T. Miller, Water Res. Research 31 (1995) 455–473.
[36] G. Mason, W.C. Clark, Chem. Eng. Sci. 20 (1965) 859–866.
[37] G. Mason, D.W. Mellor, J. Colloid Interface Sci. 176 (1995) 214–225.
[38] G.J. Mason, J. Colloid Interface Sci. 35 (1971) 279.
[39] D.W. Mellor, Ph.D. Thesis, Open University (1989).
[40] J.C. Melrose, G.C. Wallick, J. Phys. Chem. 71 (1967) 3676–3677.
[41] J.C. Melrose, SPEJ (November 1965) 259–271.
[42] K.K. Mohanty, S.J. Salter, Multiphase Flow in Porous Media: II. Pore Level Modeling, SPE Paper 11018.
[43] N.R. Morrow, N. Mungan, Rev. Inst. Fr. Petr. 26 (1971) 629–650.
[44] N.R. Morrow, P.J. Cram, F.G. McCaffery, SPEJ 255 (1973) 221–232.
[45] N.R. Morrow, Chem. Eng. Sci. 25 (1970) 1799–1815.
[46] A.D. Myshkis, V.G. Babskii, N.D. Kopachevskii, L.A. Slobozhanin, A.D. Tyuptsov, Low-Gravity Fluid Mechanics, Springer, Berlin, 1987.
[47] P.E. Øren, S. Bakke, O.J. Arntzen, SPEJ 3 (1998) 324–336.
[48] C. Pan, M. Hilpert, C.T. Miller, Water Res. Research 40 (2004) 73–91.
[49] T.W. Patzek, SPEJ 6 (2) (2001) 144–156.
[50] H. Rajaram, L.A. Ferrand, M.A. Celia, Water Res. Research 33 (1997) 43–52.
[51] P.C. Reeves, M.A. Celia, Water Res. Research 32 (1996) 2345–2358.
[52] W. Rose, J. Appl. Phys. 29 (4) (1958) 687–691.
[53] D.B. Silin, G. Jin, T.W. Patzek, Robust Determination of the Pore Space Morphology in Sedimentary Rocks, SPE 84296, SPE ATCE 2003, Denver, CO, October 5–8, 2003.
[54] D. Silverstein, T. Fort, Langmuir 16 (2000) 829–834.
[55] C. Slichter, US Geol. Surv. Ann. Rept. 306 (1899).
[56] W.O. Smith, Physics (3) (1932) 139–146.
[57] W.O. Smith, Physics (4) (1933) 425–438.
[58] W.O. Smith, Physics (4) (1933) 184–193.
[59] R. Sok, M. Knackstedt, A. Sheppard, W. Pinczewski, W. Lindquist, A. Venkatarangan, L. Paterson, Transp. Porous Media 46 (2002) 345–371.
[60] K.E. Thompson, H.S. Fogler, AIChE J. 43 (1997) 1377–1389.
[61] P.H. Valvatne, M.J. Blunt, Predictive pore-scale network modeling, SPE 84550, Proceedings of the SPE Annual Meeting, Denver, CO, 5–8 October, 2003.
[62] X. Wang, F. Thauvin, K.K. Mohanty, Chem. Eng. Sci. 54 (1999) 1859–1869.
[63] D. Wilkinson, J.F. Willemsen, J. Phys. A: Math. Gen. 16 (1983) 3365–3376.